A&A 634, A102 (2020)
https://doi.org/10.1051/0004-6361/201936912

Astronomy & Astrophysics

Star formation in outer rings of S0 galaxies

II. NGC 4513 – a multi-spin ringed S0 galaxy

I. Proshina[1], O. Sil'chenko[1], and A. Moiseev[2,1]

[1] Sternberg Astronomical Institute of the Lomonosov Moscow State University, University Av. 13, 119234 Moscow, Russia
e-mail: ii.pro@mail.ru, olga@sai.msu.su
[2] Special Astrophysical Observatory of the Russian Academy of Sciences, Nizhnij Arkhyz 369167, Russia
e-mail: moisav@gmail.com

Received 13 October 2019 / Accepted 27 December 2019

ABSTRACT

Aims. Although S0 galaxies are often thought to be "red and dead", they frequently demonstrate star formation organised in ring structures. We try to clarify the nature of this phenomenon and its difference from star formation in spiral galaxies. Here we study the moderate-luminosity nearby S0 galaxy, NGC 4513.

Methods. By applying long-slit spectroscopy along the major axis of NGC 4513, we measured gas and star kinematics, Lick indices for the main body of the galaxy, and strong emission-line flux ratios in the ring. After inspecting the gas excitation in the ring using the line ratios diagnostic diagrams and showing that it is ionised by young stars, we determined the gas oxygen abundance using popular strong-line calibration methods. We estimated the star formation rate (SFR) in the outer ring using the archival Galaxy Evolution Explorer (GALEX) ultraviolet images of the galaxy.

Results. The ionised gas counter-rotates the stars over the whole extension of NGC 4513 suggesting that it is being accreted from outside. The gas metallicity in the ring is slightly subsolar, [O/H] = −0.2 dex, matching the metallicity of the stellar component of the main galactic disc. However the stellar component of the ring is much more massive than can be explained by the current star formation level in the ring. We conclude that the ring of NGC 4513 is probably the result of tidal disruption of a massive gas-rich satellite, or may be the consequence of a long star-formation event provoked by gas accretion from a cosmological filament that started some 3 Gyr ago.

Key words. galaxies: evolution – galaxies: elliptical and lenticular, cD – galaxies: structure – galaxies: star formation

1. Introduction

Outer rings are a defining feature of S0 galaxies (de Vaucouleurs 1959). The imaging statistics reveal that about 50% of S0-S0/a galaxies possess outer stellar rings (Comerón et al. 2014; Laurikainen et al. 2011). Among those, about 50% are also seen in the UV bands (Kostiuk & Sil'chenko 2015) and therefore experience recent star formation and probably contain some amount of gas to fuel this star formation. The cool gas origin in S0s is still vague: though it is present in most S0 galaxies (Welch & Sage 2003; Sage & Welch 2006; Welch et al. 2010), its spin is often decoupled from that of the stellar component (Bertola et al. 1992; Kuijken et al. 1996; Kannappan & Fabricant 2001; Pizzella et al. 2004; Davis et al. 2011; Serra et al. 2012), especially in rarefied environments (Katkov et al. 2014, 2015), suggesting recent gas accretion from outside (Thakar & Ryden 1996, 1998). Even less is known about star formation in S0s that feature stellar ring structures: the star formation is only seen in about half of the gas-rich lenticular galaxies (Pogge & Eskridge 1993), and the conditions provoking star formation occurrence in the gas accreted by S0s are not completely understood.

In this paper we consider NGC 4513, a northern-sky (R)SA0 galaxy of moderate luminosity, $M_{\rm H} = -22.8$ (NASA/IPAC Extragalactic Database, NED). An image of the galaxy taken from the Sloan Digital Sky Survey (SDSS) DR9 (Ahn et al. 2012) is shown in the left panel of Fig. 1, and its main global parameters are given in Table 1. We previously measured the relative thickness of its stellar disc (the ratio of the vertical and radial scale lengths) using our original method, and obtained $q = 0.245 \pm 0.004$ (Chudakova & Sil'chenko 2014). The outer stellar disc of NGC 4513 is therefore somewhat thinner than the bulk of the S0 stellar discs in rarefied environments (Chudakova & Sil'chenko 2014; Sil'chenko et al. 2020) and among its morphological type (Hall et al. 2012). The galaxy is rather isolated: according to NED, there are no galaxies of comparable luminosity within 600 kpc of NGC 4513. An optical-band ring and the first spectral results for this galaxy were reported by Kostyuk (1975) and Kostyuk et al. (1981) long ago. The galaxy was observed in the 21 cm line and was found to be a rather gas-rich S0, with $0.27 \times 10^9\,M_\odot$ of the neutral hydrogen confined to the ring (Tang et al. 2008). In the Galaxy Evolution Explorer (GALEX) data, we detected a UV ring (Ilyina & Sil'chenko 2011), the radius of which is coupled to the optical ring size. A preliminary description of the spectroscopic results was presented in Ilyina et al. (2014): it was there that we found the gas in the outer ring to rotate in the opposite direction to the main stellar body. Here we present a thorough analysis of our long-slit data and of the structure of NGC 4513, including the inner part of the galaxy, as well as estimates of the star formation rate (SFR) in the outer ring obtained from imaging data in the UV retrieved from the public GALEX archive. This paper is the second in the series, which focuses on star formation

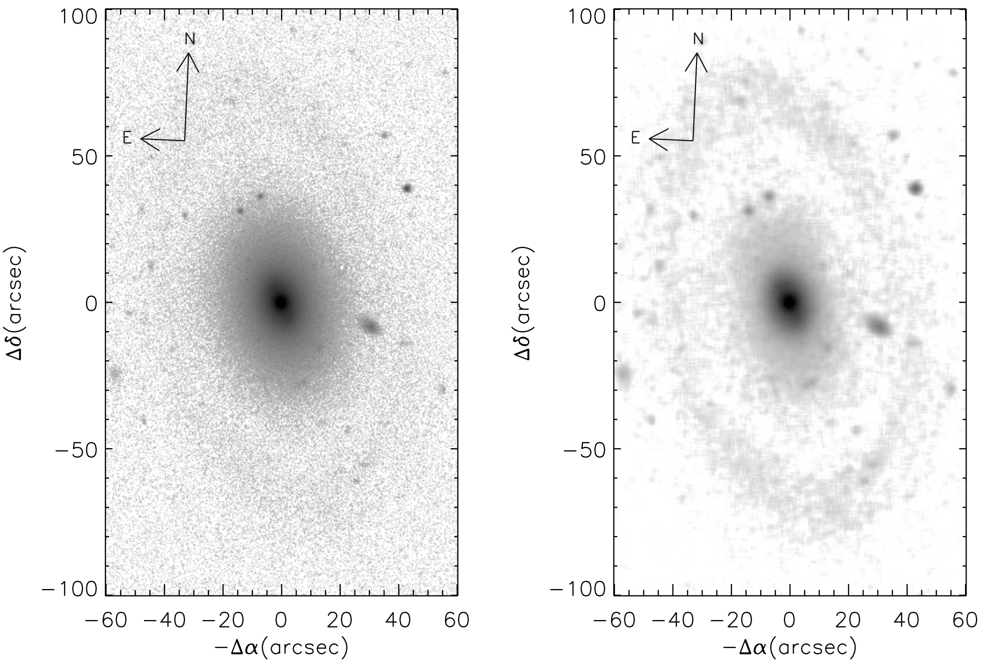

Fig. 1. The SDSS *r*-band image of NGC 4513 (*left plot*) and the same image after subtraction of the outer disc (*right plot*) – see Sect. 3 for details of the NGC 4513 image decomposition. The brightness scale is logarithmic and the same in both plots.

Table 1. Global parameters of the galaxy.

Galaxy	NGC 4513
Type (NED [1])	(R)SA0^0
R_{25} (NED+RC3 [2])	43″ or 7 kpc
B_T^0 (LEDA [3])	13.88
M_B (LEDA)	−18.99
M_H (NED)	−22.84
V_r (NED)	2304 km s^{-1}
Distance, Mpc (NED)	33
Inclination (LEDA)	59°
PA$_{phot}$ (LEDA)	15.7°
$V_{rot} \sin i$, km s^{-1} (HI [4])	∼170
σ_*, km s^{-1} (LEDA)	120
M_{HI} [4], 10^9 $M_\odot$	0.27

Notes. [1]NASA/IPAC Extragalactic Database, http://ned.ipac.caltech.edu. [2]Third Reference Catalogue of Bright Galaxies, de Vaucouleurs et al. (1991). [3]Lyon-Meudon Extragalactic Database, http://leda.univ-lyon1.fr. [4]Tang et al. (2008).

in the S0 rings; NGC 6534 and MCG 11-22-015, two galaxies with corotating detached outer rings, have previously been described by Sil'chenko et al. (2018a). As we found in our previous study of the gas kinematics in the S0 rings (Sil'chenko et al. 2019), the gas rotation in the plane coinciding with the stellar disc plane facilitates star formation. Indeed, in NGC 6534 and MCG 11-22-015 we measured SFRs of some 0.2 $M_\odot$ per year, which appears relatively high for S0 galaxies. As we show in the present paper, the counter-rotating gas of NGC 4513 on the other hand feeds much weaker star formation.

2. Observations and the data involved

Our long-slit spectral observations were made with a universal reducer, SCORPIO-2 (Afanasiev & Moiseev 2011), at the prime focus of the Russian 6 m BTA telescope of the Special Astrophysical Observatory at the Russian Academy of Sciences (SAO RAS). NGC 4513 was observed on February 8, 2011, positioning the 1″ slit along the isophote major axis, PA(slit) = 15°, with a total exposure time of 4800 s (4 × 1200 s). The seeing during these observations was poor: $FWHM \approx 3.5$ arcsec. We used the VPHG1200 grism, which has maximum effectiveness at $\lambda \approx 5400$ Å, providing an intermediate spectral resolution of $FWHM \approx 5$ Å (corresponding to an instrumental σ of 130 km s^{-1}), to obtain a spectrum over the wavelength range from 4000 to 7200 Å. This spectral range includes a set of strong absorption and emission lines making it suitable for the analysis of both the stellar and gaseous kinematics of the galaxy and its resolved stellar populations. The slit is 6′ in length which allows the edge spectra to be used to subtract the sky background. The CCD E2V CCD42-90, with a format of 2048 × 4600 px, used in the 1 × 2 binning mode provided a spatial scale of 0.357″ px^{-1} and a spectral sampling of 0.86 Å px^{-1}.

The data were reduced in a standard way using the Interactive Data Language (IDL) software package developed in the SAO RAS. At the edges of the slit we derived the sky background to subtract it from the galaxy spectra, using the polynomial (with the degree of 4) fit of the sky background distribution along the slit at every wavelength. Inhomogeneity of the optics transparency and variations of the spectral resolution along the slit were taken into account using the dawn spectrum with the high signal-to-noise ratio. The stellar kinematics were calculated by cross-correlating the binned galaxy spectra with the spectrum of HD 102328, a K2.5 giant star observed the same night as the galaxy. The emission lines, namely Hα, [NII]λ6583, [SII]λ6717,6731, and [OIII]λ5007, were used to derive ionised-gas kinematics by measuring the baricentre positions of the lines; in the bins where the continuum is strong we applied Gauss-analysis to take into account effects of underlying absorption lines: Hα as well as TiI under the [OIII]λ5007. For the latter purpose, we binned the spectra along the slit to reach a signal-to-noise ratio higher than 50–70, and then carried out a Gaussian analysis of the line complexes:

– [NII]λ6548,6583 + Hα(emission) + Hα(absorption),
– Hβ(emission) + Hβ(absorption),
– [OIII]λ5007(emission) + TiIλ5007,5015(absorption).

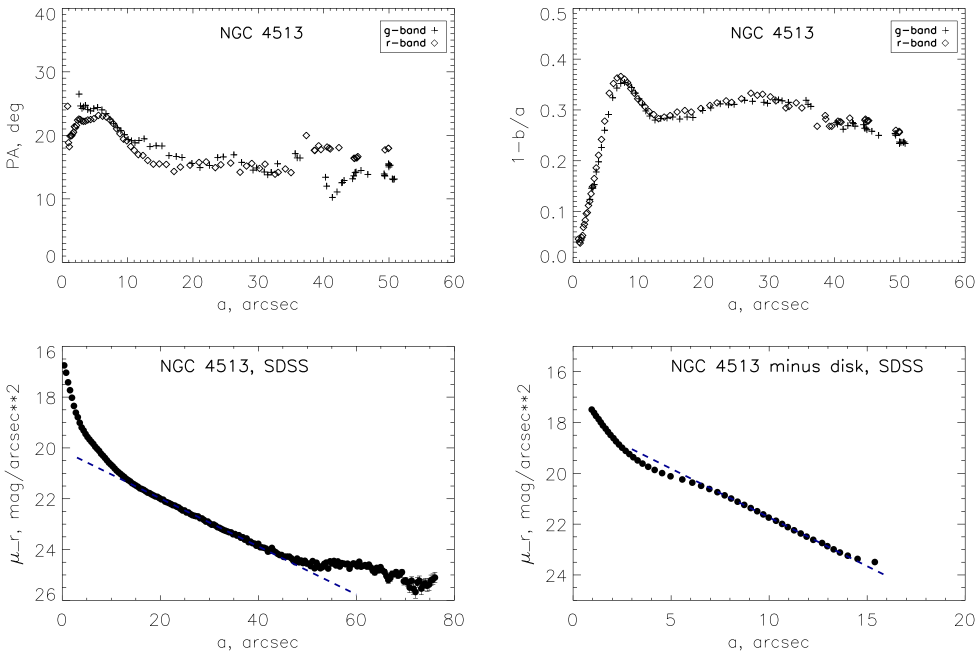

Fig. 2. Photometric analysis of the SDSS/DR9 data. Here we show the results of the isophote analysis (*upper plots*), the azimuthally averaged surface-brightness profiles of the full r-band image (*bottom left plot*), and of the image after subtraction of the outer disc (*bottom right plot*). The blue dashed lines are the fitted exponential laws showing the areas of a disc and a pseudobulge domination in NGC 4513.

With this analysis we are also able to derive the flux ratios of the strong emission lines: [NII]λ6583 to Hα, [OIII]λ5007 to Hβ, and [SII]λ6717 to [SII]λ6731, which have been used to diagnose the gas excitation mechanisms with the Baldwin-Phillips-Terlevich (BPT)-diagrams (Baldwin et al. 1981) and to determine electron density and also gas oxygen abundances for the emission-line regions where the gas is ionised by the radiation of young stars. The detector sensitivity variations along the wavelength were corrected by observing the spectrophotometric standard star, GRW+70d5824, during the same night.

To study the large-scale structure of the galaxy, we involved the g- and r-band images from the SDSS DR9 archive (Ahn et al. 2012). To estimate the SFR in the ring, we retrieved the GALEX data: NGC 4513 was deeply imaged by this space telescope on January 21, 2005, in the frame of the Guest Investigator program no. 1-045009 intended to observe another ring galaxy, VII Zw 466, projected onto the sky plane not far from NGC 4513. The total exposures of the GALEX observations were 4286 s in the far-ultraviolet (FUV) band and 8198 s in the near-ultraviolet (NUV) band.

3. Structure of NGC 4513

We carried out an isophotal analysis using the g- and r-band images of NGC 4513 provided by the SDSS/DR9 archive (Ahn et al. 2012). To this end we used the algorithm analogous to ELLIPSE/IRAF, and then by fixing the isophote parameters, the position angle (PA) of the major axis, and the ellipticity $1 - b/a$ of the outermost part of the main body of the galaxy, at $R = 15''{-}40''$, we averaged the surface brightness over the elliptical rings. The scatter of the individual ellipticity and PA measurements around the mean values in the radius range of $R = 15''{-}40''$ allows us to estimate the typical errors of $1 - b/a$ and PA in the low-surface-brightness regions; we find 0.02 and $\sim 1^\circ$, respectively. Details of our analysis of galactic exponential discs are presented in Sil'chenko et al. (2018b). The results of the isophote analysis, that is the radial profiles of the PA (major axis) and isophote ellipticity, and the surface brightness profiles, are presented in Fig. 2. The local ellipticity maximum and a turn of the isophote major axis reveal the presence of a bar ending at $R \approx 8''$. From $R \geq 14''$ to $\sim 40''$ the surface brightness profile has a perfect exponential shape, and the isophote parameters stay constant; we conclude that this is an area of large-scale exponential disc domination, since according to Freeman (1970), a defining feature of exponential stellar discs is that they obey a single-scale exponential law over the radius range of more than twice the exponential scale length. The radial scale length of the exponential profile of the outer disc of NGC 4513 is $11''.5$, or 1.8 kpc. After subtracting the model outer exponential disc from the complete r-band image of NGC 4513, we see a residual image with a rather diffuse elongated surface brightness distribution (Fig. 1, right). By constructing its azimuthally averaged surface brightness profile with ellipse aperture parameters running along the radius, we obtain an exponential profile again, with a scale length of 2.8 arcsec, or $\sim$0.5 kpc, in the radius range of $8{-}14''$ (Fig. 2, bottom right). We conclude that the bulge of NGC 4513 is in fact a pseudobulge, and as the stellar system is dynamically cold, this also includes a bar. Figure 1 shows a surface brightness excess in the radius range of $55{-}72''$, and it is also seen in the full surface brightness profile in the bottom left panel of Fig. 2; this is a signature of an outer stellar ring at the radius of about 10–12 kpc, beyond the outer edge of the main stellar disc, $R_{25} = 43''$, or 7 kpc (de Vaucouleurs et al. 1991).

4. Counter-rotating gas and a complex stellar component in NGC 4513

The top plot of Fig. 3 presents the line-of-sight velocity variations along the slit for the stars and ionised gas in NGC 4513. The velocities of the stellar component were determined by cross-correlating galaxy spectra with the spectrum of a K-giant star observed the same night with the same spectrograph configuration. The velocities of the ionised gas in the central part of the galaxy, $R < 10''$, were measured by Gaussian analysis of the line blends including the underlying absorption lines. In the outermost part of the main disc, that is, the northern part where the continuum is faint, we calculated the baricentre wavelength

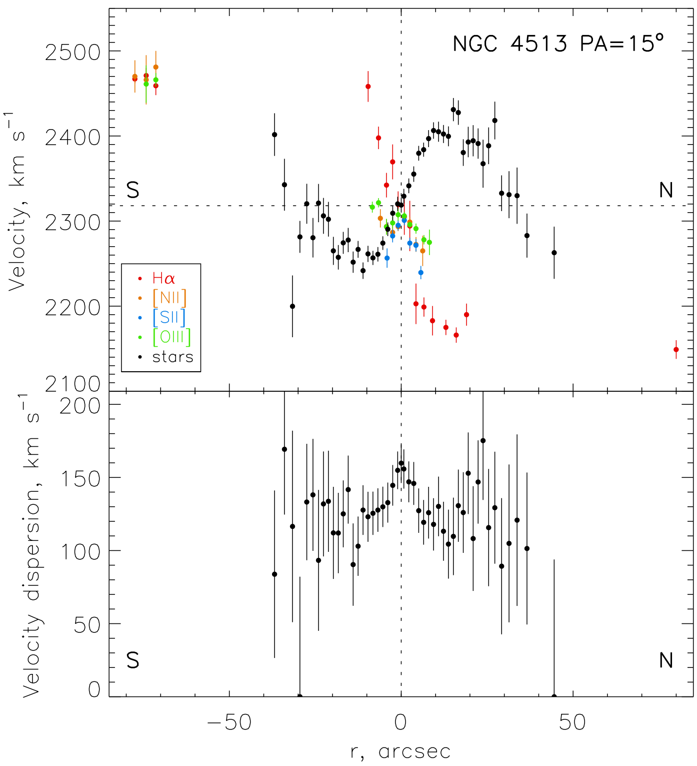

Fig. 3. Line-of-sight velocity profiles for the ionised gas and stars (*top*) and the stellar velocity dispersion profile (*bottom*) in NGC 4513 along its major axis. The black signs show the stellar component while various coloured signs refer to different emission lines of the ionised gas.

position for Hα at every radius. As Fig. 3 demonstrates, the ionised gas rotates in the opposite direction to the stars over most of the galaxy. The stellar rotation curve starts to fall beyond $R \approx 15''$ and switches into a counter-rotating regime at the outer edge of the disc, at $R \geq 30''$. This suggests the possible existence of a secondary stellar component which may be related to the gas. Its presence may result in superposition of two counter-rotating stellar components giving a null average rotation velocity at $R \approx 25''$ within the photometric disc-dominated area. To test this possibility, we plotted a profile of the measured stellar velocity dispersion estimated as a σ of the stellar line-of-sight velocity distribution (LOSVD) (Fig. 3, bottom). Though our spectral resolution does not allow us to reliably measure stellar velocity dispersions below 100 km s^{-1} expected in a disc, we are still able to see a qualitative increase of the visible stellar velocity dispersion after the reverse of the rotation curve. Such behaviour of the stellar velocity dispersion profile supports our hypothesis that there are two stellar-rotation components at our line of sight in the disc-dominated area. The rotation of the ionised gas in NGC 4513 is traced by measuring four strong emission lines (Fig. 3). In the central part of the galaxy, at $R < 10''$, we see a rather flat segment of the gaseous velocity profile, consistent with a suggested gas slowdown at the bar edges. The gas rotation curve rises steeply further into the pseudobulge area until its border at $R \approx 10''$. The gas velocities in the ring, being equal to the gas velocities at $|R| = 10''-15''$, imply a flat shape of the circular rotation curve over the full extension of the NGC 4513 disc. We do not see any emission lines between the inner edge of the disc and the outer ring, which is in line with the discovery by Tang et al. (2008) of a prominent central depression in the HI distribution.

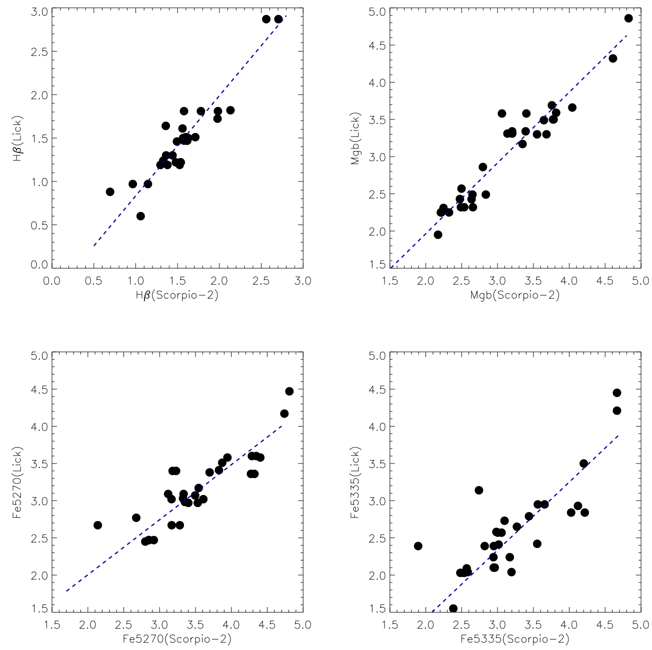

Fig. 4. Linear calibration of our instrumental Lick indices vs. standard Lick indices for a sample of bright stars from Worthey et al. (1994).

5. Stellar population properties

To analyse the ages and chemical composition of the NGC 4513 stellar population, we calculated the Lick indices Hβ, Mgb, Fe5270, and Fe5335, as well as the combined iron index, $\langle \mathrm{Fe} \rangle \equiv (\mathrm{Fe5270} + \mathrm{Fe5335})/2$, and combined metallicity index, $[\mathrm{MgFe}] \equiv \sqrt{\mathrm{Mgb}\langle \mathrm{Fe} \rangle}$, along the radius using our long-slit spectrum obtained with SCORPIO-2 of the Russian 6 m telescope. We favour the Lick index analysis here because we expect a non-solar ratio of the α-element-to-iron abundances, and the currently popular full-spectral-fitting method is still restricted to the assumption of a solar element pattern. Firstly, we calibrated our SCORPIO-2 index system to the standard Lick one by observing several standard stars from the Worthey et al. (1994) sample. The linear calibration dependencies are presented in Fig. 4. The scatter of individual stars around the linear dependencies, namely ~0.2 Å, is comparable to the accuracy of the Lick index measurements by Worthey et al. (1994).

We then estimated the SSP-equivalent ages and metallicities of the stellar populations along the radius of NGC 4513 by comparing our measurements of the Lick indices with the evolutionary synthesis models by Thomas et al. (2003). The Hβ index was corrected for the emission contamination in the innermost part of the galaxy through measuring the Hα emission-line equivalent width as described in Sil'chenko (2006). Subsequently, broad radial bins were defined that correspond to the photometric borders of the unresolved nucleus, $R < 4''$, the bar, $R = 4-8''$, the pseudobulge, $R = 8-14''$, and the large-scale stellar disc, $R = 14-40''$. Our Lick indices were averaged within these radial bins. The results are presented in Fig. 5. The central part of the galaxy is homogeneously old and shows an overabundance of magnesium. However, the large-scale stellar disc of NGC 4513 differs from the centre of the galaxy in terms of the properties of its stellar population: it shows a more prolonged history of star formation (its magnesium-to-iron ratio is closer to the solar value), which stopped only a few billion years ago. The stellar metallicity of the galactic disc is only slightly subsolar. It is rather unusual for the outer stellar discs of lenticular

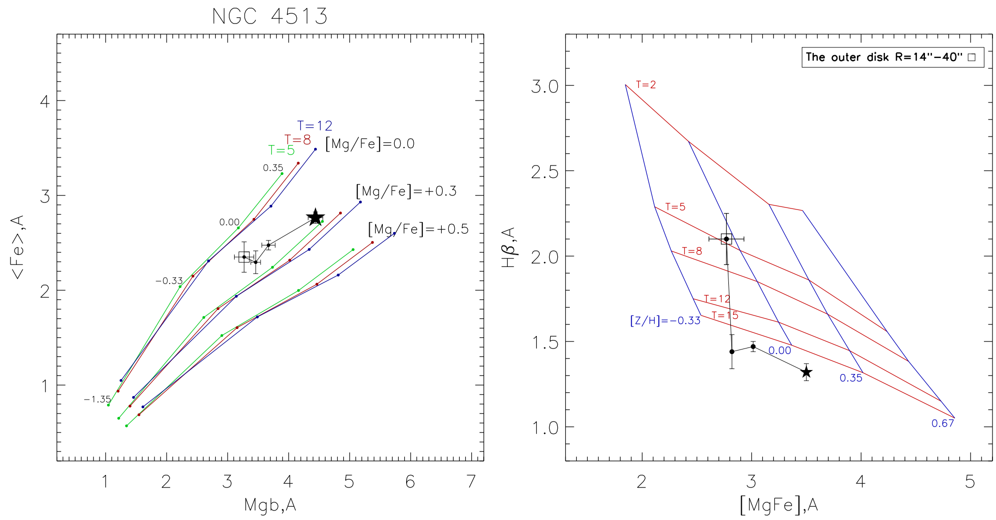

Fig. 5. Lick index-index diagrams for NGC 4513. *Left plot*: magnesium vs. iron index diagram which allows us to estimate a magnesium-to-iron ratio through the comparison of our measurements with the models by Thomas et al. (2003) for the different Mg/Fe ratios. By comparing the Hβ Lick index with a combined metallicity Lick index involving magnesium and iron lines (*right plot*), we solve the metallicity–age degeneracy and determine these stellar population parameters with the SSP evolutionary synthesis models by Thomas et al. (2003). Five different age sequences (red lines) are plotted as a reference frame; the blue lines crossing the model age sequences mark the metallicities of +0.67, +0.35, 0.00, and −0.33 from right to left. A large black star corresponds to the central core, $R < 4''$, and then we go along the radius through the galaxy structure components: $R = 4''-8''$ (bar), $R = 8''-14''$ (pseudobulge), and $R = 14''-40''$ (disc). The point corresponding to the outer stellar disc is outlined by a large square.

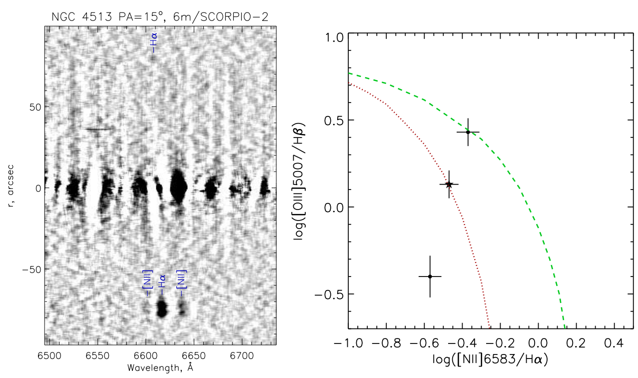

Fig. 6. Emission lines in the spectrum of NGC 4513: Hα and the [NII] doublet (*left*) and the BPT-diagram for the southern tip of the ring (*right*). At the BPT-diagram the known boundaries between HII-region excitation type and the others are plotted: the green dashed line is a theoretical boundary by Kewley et al. (2001), and the dotted red line is an empirical star-formation sequence from Kauffmann et al. (2003). We have plotted separately the inner edge of the ring, $R = 71.5''$ (upper dot), and the outer edge of the ring, $R = 76.5''$ (lower dot). The whole (integrated) ring is shown by a black star.

galaxies in a rarefied environment which are known to be coeval with their bulges (Katkov et al. 2015), or to be older (Sil'chenko et al. 2012). We may also relate this unusual stellar age distribution to the presence of the secondary, probably young stellar component which has come into the outer disc of NGC 4513 with the counter-rotating gas accretion.

6. Gas-phase metallicity

The left panel of Fig. 6 shows the emission-line long-slit spectrum of NGC 4513 along its major axis, namely its red portion with the continuum subtracted, and the right panel of Fig. 6 shows the BPT diagram for the southernmost location of the emission lines. One can clearly see gas–star counter-rotation as well as the absence of emission lines between the central part of NGC 4513 and its star-forming ring which demonstrates emission lines in the radius range of $R = 70-80''$.

The emission line Hα is weak throughout the central part of NGC 4513, and the strongest emission line is [NII]λ6583. Such a line ratio is consistent with possible gas excitation by old stars (Binette et al. 1994; Byler et al. 2019), which is in agreement with the age of the stellar population in the central part of NGC 4513 (see Sect. 5). Alternatively, the gas within $R < 8''$ could be excited by a shock mechanism which is consistent with the presence of a bar. The bar contribution to the gas excitation may also account for the strongly asymmetric electron density distribution along the slit: we measured the trend of the sulfur line ratio, [SII]6717/6731, from 0.71 ± 0.07 south of the nucleus to 1.13 ± 0.04 north of the nucleus, which corresponds to a n_e difference of about an order: 2400 cm^{-3} versus 300 cm^{-3} respectively (Kewley et al. 2019).

In the ring, the situation concerning the source of gas ionisation could be different: here we expected gas excitation by current star formation. We plotted the emission-line ratios in the southern tip of the ring onto the BPT diagram (Fig. 6, right). Indeed, the strong line ratios in the ring of NGC 4513 appear to lie below the theoretical border of star formation calculated by Kewley et al. (2001), and therefore the ionised gas of the ring may be mostly excited by young stars. However, the prominent offset of the inner edge of the ring in the BPT diagram with respect to the observational star formation sequence by Kauffmann et al. (2003) places this region in the so-called "composite zone", revealing a noticeable contribution of diffuse interstellar gas (DIG) or shocks to the spectrum of the ionised gas of the ring. This means that not all strong-line methods of gas oxygen determination are applicable to the inner edge of the ring in NGC 4513. Recent studies have shown that in the presence of DIG the most reliable metallicity calibration is provided by the O3N2 method (Kumari et al. 2019). Exploring both O3N2 calibrations from Pettini & Pagel (2004) and Marino et al. (2013), we obtained

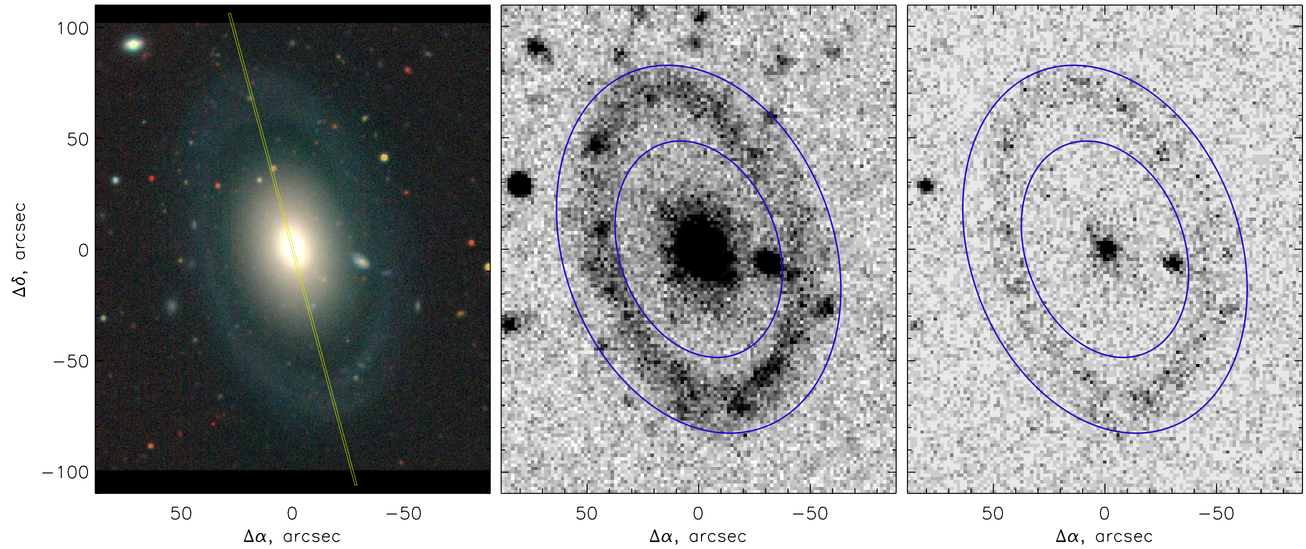

Fig. 7. Optical composite-colour image (*left*), the product of the BASS survey, taken from the Legacy Survey website (`http://legacysurvey.org`). The SCORPIO-2 slit position is overlapped. Also shown are the GALEX maps (NUV, *middle*, and FUV, *right*) of NGC 4513 with the apertures for the SFR estimates in the ring overplotted.

$12 + \log(O/H) = 8.42 \pm 0.06$ dex for the inner edge of the ring of NGC 4513. For the outer edge of the ring, which is inside the HII-region area of the BPT diagram, and for the whole ring, which falls exactly onto the star formation sequence by Kauffmann et al. (2003), we used both N2 and O3N2 methods from the papers by Pettini & Pagel (2004) and Marino et al. (2013). We obtained $12 + \log(O/H) = 8.57 \pm 0.06$ dex for the outer edge of the ring and $12 + \log(O/H) = 8.54 \pm 0.06$ dex for the whole ring. Together with the inner edge of the ring, these estimates imply a gas ring metallicity of about −0.2 dex with respect to solar metallicity. This matches rather closely the stellar metallicity of the large-scale disc of NGC 4513 as reported in Sect. 5. Comparison of the gas oxygen abundance in NGC 4513 to that of other outer rings of S0s (Proshina et al. 2019; Sil'chenko et al. 2019) reveals exactly the same metallicity: for a sample of a dozen gaseous outer rings in S0s, mostly with corotating kinematics (though in NGC 2551 the gas counter-rotates), we find $\langle[O/H]\rangle = -0.15$ dex (Sil'chenko et al. 2019).

7. Star formation in the outer ring of NGC 4513

NGC 4513 was observed by the UV space telescope GALEX. Relatively large exposure times allowed us to obtain deep FUV and NUV images of the galaxy, with particular emphasis on the outer ring (Fig. 7). We retrieved these FUV and NUV images from the Mikulski Archive for Space Telescope (MAST) Archive and superimposed an elliptical-ring aperture that is slightly broader than the ring itself in order to include all of the ultraviolet flux, with the ellipticity matching the galaxy inclination, $1 - b/a = 0.3$. The aperture is centred on the NGC 4513 nucleus. It is aligned with the outer isophote major axis and has an inner radius of 50″ and an outer radius of 85″ (Fig. 7). We then integrated the FUV and NUV fluxes within this ring aperture. The surrounding background was measured and subtracted. The fluxes in counts were re-calculated into FUV and NUV magnitudes using the procedures described by Morrissey et al. (2007). We then corrected them for the foreground Galactic extinction by taking the NED A_B data for NGC 4513, and transformed them into FUV and NUV luminosities using the NED-provided distance of 33 Mpc to NGC 4513. We applied the correction for the intrinsic dust using the WISE/Band 4 (22 μm) image of NGC 4513 cut with the same elliptic-ring aperture. By obtaining the FUV and NUV luminosities of the ring, we transformed them into SFRs averaged over the last 100 and 200 Myr, respectively, using the calibrations proposed by Kennicutt & Evans (2012).

The resulting SFR estimate for the ring of NGC 4513 is 0.026 solar masses per year (0.022 $M_\odot$ yr^{-1} from the FUV data and 0.030 $M_\odot$ yr^{-1} from the NUV data). We compared this SFR with the total stellar mass of the NGC 4513 ring. Indeed, the SDSS data allow us to estimate the integrated g-band and r-band magnitudes of the ring (in the same elliptical-ring aperture as the UV signals): $g(\text{ring}) = 15.16$ and $r(\text{ring}) = 14.61$. With the distance to NGC 4513 of 33 Mpc, we derived the absolute magnitude of the ring: $M_g(\text{ring}) = -17.4$. Using the Bell et al. (2003) calibration of the mass-to-luminosity ratio against the colour, with $g - r(\text{ring}) = 0.55$ we obtain $M/L_g = 2.14$, and therefore the total stellar mass of the ring is $2.26 \times 10^9\ M_\odot$.

Now we can test the different scenarios of star formation history in the ring. To accumulate a stellar mass of $2.26 \times 10^9\ M_\odot$ with a constant SFR in the ring of 0.026 $M_\odot$ yr^{-1} – the rate that we found from the UV signal for the last 100−200 Myr, – the galaxy requires much more than the Hubble time. Under the opposite scenario, if the star formation history (the SFH) declined exponentially and started approximately 3 Gyr ago, we would obtain the same stellar mass with an e-folding time of 0.6 Gyr, which is typical for the S0 outer ring SFH (Proshina et al. 2019). In the former scenario we must conclude that not only has the gas been accreted from outside, but a substantial amount of the stellar mass has been accreted as well. In this case we deal not with pure gas accretion, but with tidal disruption of a gas-rich satellite. In the latter scenario, the galaxy can accrete only cold gas, but the mass of this gas, which is about $2.5 \times 10^9\ M_\odot$, constitutes more than 10% of the total stellar mass of NGC 4513. The invisible source of the counter-rotating gas in this case must be extremely abundant. In principle, it can be accretion of primeval gas from a cosmological filament because the current ratio of stellar-to-gas mass in the ring, which is approximately 8:1, places the chemical evolution of the ring of NGC 4513 in the "gas-depleted" stage (Zahid et al. 2014; Ascasibar et al. 2015), meaning that the current metallicity of the ionised gas must correspond to the saturation level, which is close to the solar value (Zahid et al. 2014; Ascasibar et al. 2015), independently of the initial gas metallicity. This may explain the proximity of the gas oxygen abundance in the ring of NGC 4513 to the common value found by us for a number of other outer rings in S0 galaxies (Sil'chenko et al. 2019).

8. Discussion and conclusion: the origin of the ring in NGC 4513

Although NGC 4513 has a small bar according to our photometric analysis results (Fig. 2), we do not think that its outer ring is related to the resonances of the bar. Indeed, rings at outer Lindblad resonances show typical radii of 1.5–2 bar radii (Buta 2017), while in NGC 4513, $R(\text{ring})/R(\text{bar}) = 10 \pm 2$. Furthermore, the gas content of the ring rotates in the opposite direction to the main stellar body of the galaxy, providing unambiguous evidence of accretion by the ring.

Moreover, star formation in the ring is weak, that is $0.026\,M_{\odot}\,\text{yr}^{-1}$, over a timescale of approximately 100 Myr. If this SFR has remained roughly constant, then the stellar content of the ring, namely $2.3 \times 10^{9}\,M_{\odot}$, could not have been formed in situ and must have been accreted together with the gas. If the SFR in the ring has strongly declined on the other hand, with an e-folding time of $\sim$0.6 Gyr during the last 3 Gyr, then the stellar content of the ring could have been formed in situ. The latter scenario implies that the stellar ring of NGC 4513 may be a consequence of a long star-formation event provoked perhaps by gas accretion from a cosmological filament, as in the ring-like Hoag galaxy (Finkelman et al. 2011). In any case, the stars related to the counter-rotating gas may contribute to the outer stellar disc of NGC 4513, which displays SSP-equivalent stellar ages of less than 5 Gyr together with a sharply falling rotation curve. The most probable scenario of ring acquisition by NGC 4513 is one of tidal disruption of a gas-rich satellite. The ratio of $\log M_{\text{HI}}/M_{*} \geq -0.9$, which we found for the outer ring of NGC 4513, is indeed typical for satellite galaxies in gas-rich loose groups (Dzudzar et al. 2019). The environment of NGC 4513 corresponds to this scenario: according to the NED, the galaxy is relatively isolated and belongs to a loose group of four galaxies. Its currently nearest neighbour, the emission-line dwarf PGC 2683704, is at 270 kpc and is less massive by a factor of 30. We suggest that a similar but closer satellite was disrupted at some point by NGC 4513 and formed a ring with a radius corresponding to its orbital momentum.

Acknowledgements. We are grateful to the anonymous referee who has made a lot of very useful comments resulting in the paper improvement. The study of galactic rings was supported by the Russian Foundation for Basic Researches, grant no. 18-02-00094a. The work is based on the data obtained at the Russian 6 m telescope of the Special Astrophysical Observatory carried out with the financial support of the Ministry of Science and Higher Education of the Russian Federation and on the public data of the SDSS (`http://www.sdss3.org`) and GALEX (`http://galex.stsci.edu/GR6/`) surveys. The NASA GALEX mission data were taken from the Mikulski Archive for Space Telescopes (MAST). The WISE data exploited by us were retrieved from the NASA/IPAC Infrared Science Archive, which is operated by the Jet Propulsion Laboratory, California Institute of Technology, under contract with the National Aeronautics and Space Administration. The NGC 4513 composite-colour optical image was taken from the Legacy Survey collection providing the imaging data of the BASS survey. BASS is a key project of the Telescope Access Program (TAP), which has been funded by the National Astronomical Observatories of China, the Chinese Academy of Sciences (the Strategic Priority Research Program "The Emergence of Cosmological Structures" Grant no. XDB09000000), and the Special Fund for Astronomy from the Ministry of Finance. The BASS is also supported by the External Cooperation Program of Chinese Academy of Sciences (Grant no. 114A11KYSB20160057), and Chinese National Natural Science Foundation (Grant no. 11433005). The Legacy Surveys imaging of the DESI footprint is supported by the Director, Office of Science, Office of High Energy Physics of the US Department of Energy under Contract No. DE-AC02-05CH1123, by the National Energy Research Scientific Computing Center, a DOE Office of Science User Facility under the same contract; and by the US National Science Foundation, Division of Astronomical Sciences under Contract No. AST-0950945 to NOAO.

References

Afanasiev, V. L., & Moiseev, A. V. 2011, Balt. Astron., 20, 363
Ahn, C. P., Alexandroff, R., Allende Prieto, C., et al. 2012, ApJS, 203, 21
Ascasibar, Y., Gavilán, M., Pinto, M., et al. 2015, MNRAS, 448, 2126
Baldwin, J. A., Phillips, M. M., & Terlevich, R. 1981, PASP, 93, 5
Bell, E. F., McIntosh, D. H., Katz, N., & Weinberg, M. D. 2003, ApJS, 149, 289
Bertola, F., Buson, L. M., & Zeilinger, W. W. 1992, ApJ, 401, L79
Binette, L., Magris, C. G., Stasińska, G., & Bruzual, A. G. 1994, A&A, 292, 13
Buta, R. J. 2017, MNRAS, 470, 3819
Byler, N., Dalcanton, J. J., Conroy, C., et al. 2019, AJ, 158, 2
Chudakova, E. M., & Sil'chenko, O. K. 2014, Astron. Rep., 58, 281
Comerón, S., Salo, H., Laurikainen, E., et al. 2014, A&A, 562, A121
Davis, T. A., Alatalo, K., Sarzi, M., et al. 2011, MNRAS, 417, 882
de Vaucouleurs, G. 1959, Handb. Phys., 53, 275
de Vaucouleurs, G., de Vaucouleurs, A., Corwin, Jr., H. G., et al. 1991, Third Reference Catalogue of Bright Galaxies (Berlin, Heidelberg, New York: Springer-Verlag)
Dzudzar, R., Kilborn, V., Meurer, G., et al. 2019, MNRAS, 483, 5409
Finkelman, I., Moiseev, A., Broash, N., & Katkov, I. 2011, MNRAS, 418, 1834
Freeman, K. C. 1970, ApJ, 160, 767
Hall, M., Courteau, S., Dutton, A. A., et al. 2012, MNRAS, 425, 2741
Ilyina, M. A., & Sil'chenko, O. K. 2011, Astron. Lett., 37, 589
Ilyina, M. A., Sil'chenko, O. K., & Afanasiev, V. L. 2014, MNRAS, 439, 334
Kannappan, S. J., & Fabricant, D. G. 2001, AJ, 121, 140
Katkov, I. Yu., Sil'chenko, O. K., & Afanasiev, V. L. 2014, MNRAS, 438, 2798
Katkov, I. Yu., Kniazev, A. Yu., & Sil'chenko, O. K. 2015, AJ, 150, 24
Kauffmann, G., Heckman, T. M., Tremonti, Ch., et al. 2003, MNRAS, 346, 1055
Kennicutt, Jr., R. C., & Evans, II, N. J. 2012, Annu. Rev. Astron. Astrophys., 50, 531
Kewley, L. J., Dopita, M. A., Sutherland, R. S., Heisler, C. A., & Trevena, J. 2001, ApJ, 556, 121
Kewley, L. J., Nicholls, D. C., Sutherland, R. S., et al. 2019, ApJ, 880, 16
Kostiuk, I. P., & Sil'chenko, O. K. 2015, Astrophys. Bull., 70, 280
Kostyuk, I. P. 1975, Soobscheniya Spets. Astrofiz. Obs., 13, 45 [in Russian]
Kostyuk, I. P., Karachentsev, I. D., & Kopylov, A. I. 1981, Sov. Astron. Lett., 7, 148
Kuijken, K., Fisher, D., & Merrifield, M. R. 1996, MNRAS, 283, 543
Kumari, N., Maiolino, R., Belfiore, F., & Curti, M. 2019, MNRAS, 485, 367
Laurikainen, E., Salo, H., Buta, R., & Knapen, J. H. 2011, MNRAS, 418, 1452
Marino, R. A., Rosales-Ortega, F. F., Sánchez, S. F., et al. 2013, A&A, 559, A114
Morrissey, P., Conrow, T., Barlow, T. A., et al. 2007, ApJS, 173, 682
Pettini, M., & Pagel, B. E. J. 2004, MNRAS, 348, L59
Pizzella, A., Corsini, E. M., Vega Beltrán, J. C., & Bertola, F. 2004, A&A, 424, 447
Pogge, R. W., & Eskridge, P. B. 1993, AJ, 106, 1405
Proshina, I. S., Kniazev, A. Yu., & Sil'chenko, O. K. 2019, AJ, 158, 5
Sage, L. J., & Welch, G. A. 2006, ApJ, 644, 850
Serra, P., Oosterloo, T., Morganti, R., et al. 2012, MNRAS, 422, 1835
Sil'chenko, O. K. 2006, ApJ, 641, 229
Sil'chenko, O. K., Proshina, I. S., Shulga, A. P., & Koposov, S. E. 2012, MNRAS, 427, 790
Sil'chenko, O., Kostiuk, I., Burenkov, A., & Parul, H. 2018a, A&A, 620, L7
Sil'chenko, O. K., Kniazev, A. Yu., & Chudakova, E. M. 2018b, AJ, 156, 118
Sil'chenko, O. K., Moiseev, A. V., & Egorov, O. V. 2019, ApJS, 244, 6
Sil'chenko, O. K., Kniazev, A. Yu., & Chudakova, E. M. 2020, AJ, submitted
Tang, Y.-W., Kuo, Ch.-Y., Lim, J., & Ho, P. T. P. 2008, ApJ, 679, 1094
Thakar, A. R., & Ryden, B. S. 1996, ApJ, 461, 55
Thakar, A. R., & Ryden, B. S. 1998, ApJ, 506, 93
Thomas, D., Maraston, C., & Bender, R. 2003, MNRAS, 339, 897
Welch, G. A., & Sage, L. J. 2003, ApJ, 584, 260
Welch, G. A., Sage, L. J., & Young, L. M. 2010, ApJ, 725, 100
Worthey, G., Faber, S. M., González, J. J., & Burstein, D. 1994, ApJS, 94, 687
Zahid, H. J., Dima, G. I., Kudritzki, R.-P., et al. 2014, ApJ, 791, 130